

# Light scattering under nanofocusing: Towards coherent nanoscopies

Ahmad Mohammadi<sup>a</sup>, Mario Agio<sup>b</sup>

<sup>a</sup>*Department of Physics, Persian Gulf University, 75196 Bushehr, Iran*

<sup>b</sup>*Laboratory of Physical Chemistry, ETH Zurich, 8093 Zurich, Switzerland*

## Abstract

We investigate light scattering under nanofocusing in the context of coherent spectroscopy. We discuss the different mechanisms that may enhance the signal in extinction and how these depend on nanofocusing as well as on the probed system. We find that nanofocusing may improve the detection sensitivity by orders of magnitude under realistic conditions, enabling scanning implementations of coherent spectroscopy at the nanoscale.

**Keywords:** nanofocusing, coherent spectroscopy, light-matter interaction, scanning-probe technology

## 1. Introduction

Optical nanoscopy is recognized as a powerful tool for investigating physico-chemical as well as biological processes in nanomaterials, whereby subwavelength spatial resolution is combined with a variety of spectroscopic techniques. The past decades have witnessed the development of several successful attempts in this regard, such as scanning near-field optical microscopy (SNOM) [1–5], single-molecule spectroscopy [6–10] and the combination of the two [11–14]. These efforts have however suffered from the mismatch between light and nanoscale matter, which leads to a small throughput between the input and output signals. That is why coherent detection schemes, whereby input and output are in a well defined phase relationship, have found less application, although they may provide additional information [15–18].

Recent developments in single-molecule spectroscopy have however been able to push the limits of coherent detection under various conditions [19–23]. On the theoretical side, it has been found that there is a profound relationship between the optimal concentration of electromagnetic energy and the strength of light-matter interaction [24, 25], pointing out how the possibility of focusing light below the diffraction limit may enhance the detected signal. The immediate question that arises is thus how to improve these schemes further and how to implement them for optical nanoscopies.

To address these questions we first note that the dramatic advances of nanotechnology experienced in recent years have enabled us to fabricate optical nanostructures that greatly improve the conversion of localized electromagnetic energy into radiation and vice versa [26–28]. In this context, single-molecule studies have shown how these so-called optical antennas may provide an unprecedented control over molecular fluorescence [29–33].

Recently, it has been found that a truncated metal nanocone may focus light into nanoscale dimensions with minimal suffering from absorption losses [34] and modify the radiation pattern of a light emitter placed near its tip [35]. Furthermore, such antenna architecture is fully compatible with scanning probe technology [36]. Nanofocusing relies on the propagation of surface plasmon polaritons (SPPs) along a metal nanowire [37]. These modes do not have a cut-off and propagate optical energy in a tapered structure up to the very end [38, 39]. Note that this phenomenon applies to a variety of waveguide geometries [40].

Our aim is to combine coherent spectroscopy with nanofocusing to explore how this approach may expand the detection limits of nanoscale objects, with particular attention on the competition between the enhancement of light-matter interaction, coherent detection as well as damping and dephasing processes. We furthermore highlight the unique features of scattering under nanofocusing and derive expressions for the visibility and the phase shift caused by a point-like polarizable object placed in the near-field of the nanocone sharp end. We verify our ideas by means of rigorous electrodynamic calculations, choosing very small metal particles to model nanoscale emitters affected by strong non-radiative damping.

## 2. Formulation

### 2.1. Coherent scattering under focusing

Textbook treatments of coherent scattering consider a polarized plane wave incident on a material object. Under these assumptions we may take advantage of the optical theorem to relate the signal collected by an infinitesimal detector placed in the forward direction to the total amount of power  $P_{\text{ext}}$  removed from the beam by the obstacle [41]. If  $P_{\text{inc}}$  is the incident power, the normalized detected signal reads

$$S = 1 - P_{\text{ext}}/P_{\text{inc}} = 1 - V, \quad (1)$$

where  $V$  stands for visibility. An established approach to enhance  $V$  relies on focusing light. However, because the optical

Email address: mario.agio@phys.chem.ethz.ch (Mario Agio)

theorem fails when the incident wave is not plane [42], we need to depart from Eq. (1) and consider the scattering problem from first principles.

Figure 1a sketches the typical arrangement of an extinction experiment where the incident field  $E_{\text{inc}}$  is focused by a lens and the output field  $E_{\text{out}}$  is collected by another lens placed in the forward direction. According to scattering theory,  $E_{\text{out}}$  corresponds to the sum of the incident and scattered fields. Moreover, since we are interested in nanoscale objects, we may say that the scattered field  $E_{\text{sca}}$  is proportional to the dipolar polarizability  $\alpha$  and  $E_{\text{inc}}(O)$ , the incident field at the focal spot  $O$ . For a classical oscillating dipole and a weakly excited quantum emitter we find [43, 44]

$$\alpha = -\frac{6\pi}{k^3} \frac{\Gamma_1}{2\Delta + i\Gamma_2}, \quad (2)$$

where  $k$  is the wavevector,  $\Delta$  is the detuning from resonance and  $\Gamma_1, \Gamma_2$  respectively are the radiative and total damping rates.

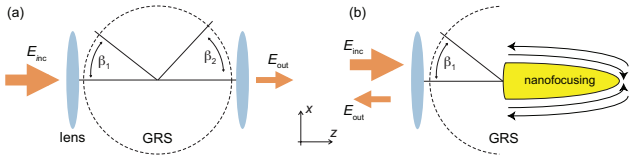


Figure 1: Coherent spectroscopy under focusing (a) and nanofocusing (b).  $\beta_1$  and  $\beta_2$  are the focusing and collection semi-angles, respectively. Note that in (b) focusing and collection occur through the same objective. The dashed circle sketches the Gaussian reference sphere (GRS). The black curves in (b) depict the propagation of SPPs in both directions.

In free space there is a fundamental limit to the optimal concentration of electromagnetic energy [45]. To understand how this gives rise to an upper bound for  $V$ , we assume that  $E_{\text{inc}}$  is a focused plane wave of amplitude  $E_o$ . Furthermore, we explicitly consider the dependence on the focusing and collection semi-angles. In these circumstances Eq. (1) is replaced by

$$S = 1 + \chi(\beta_2) P_{\text{sca}}/P_{\text{inc}} + \int_0^{\Omega_{\beta_2}} 2\text{Re}\{E_{\text{inc}} E_{\text{sca}}^*\} d\Omega / P_{\text{inc}}, \quad (3)$$

where  $d\Omega$  is the infinitesimal collection solid-angle, whose maximum is  $\Omega_{\beta_2}$ , and  $\chi(\beta_2) = (4 - 3\cos\beta_2 - \cos^3\beta_2)/8$  [24].

If  $\sigma_{\text{sca}} = k^4 |\alpha|^2 / 6\pi$  is the scattering cross section [41], the scattered power reads

$$P_{\text{sca}} = \sigma_{\text{sca}} \frac{k^2 |E_o|^2 f^2}{4} \mathcal{I}_o^2(\beta_1), \quad (4)$$

where  $f$  is the lens focal length and  $\mathcal{I}_o(\beta_1)$  is the diffraction integral

$$\mathcal{I}_o(\beta_1) = \int_0^{\beta_1} d\theta \sin\theta \sqrt{\cos\theta} (1 + \cos\theta). \quad (5)$$

The third term at the right side of Eq. (3) represents the power  $P_{\text{int}}$  associated with the interference between  $E_{\text{inc}}$  and  $E_{\text{sca}}$ . For  $\beta_2 > \beta_1$  we find

$$P_{\text{int}} = -\sigma_{\text{ext}} \frac{k^2 |E_o|^2 f^2}{4} \mathcal{I}_o^2(\beta_1). \quad (6)$$

Note that  $P_{\text{int}}$  is negative and contains the so-called extinction cross section  $\sigma_{\text{ext}} = k\text{Im}\{\alpha\}$  [41]. It corresponds to  $P_{\text{ext}}$  for plane-wave scattering. Moreover,  $|\mathcal{I}_o(\beta_1)|^2$  stems from two contributions. One comes from  $E_{\text{sca}}$ , since  $E_{\text{inc}}(O) \propto \mathcal{I}_o(\beta_1)$ . The other one comes from the collection integral in Eq. (3). That explains how the visibility  $P_{\text{int}}/P_{\text{inc}}$  builds up, showing that it depends twice on a diffraction integral: first in the focusing process, second in the collection process. Equations (4) and (6) are valid for any type of focused beam if we replace  $k^2 f^2 |E_o|^2 |\mathcal{I}_o(\beta_1)|^2 / 4$  with  $2cW_{\text{inc}}(O)^{(\text{el})}$ , where  $c$  is the speed of light and  $W_{\text{inc}}(O)^{(\text{el})}$  is the electric energy density at the focal spot [24].

## 2.2. Visibility

The maximum of  $V$  is easily obtained starting from the Bassett limit [45]

$$W_{\text{inc}}^{(\text{el})}(O)/P_{\text{inc}} \leq k^2/(6\pi c) \quad (7)$$

and from the fact that an ideal oscillating dipole yields  $\sigma_{\text{ext}} = \sigma_{\text{sca}} = \sigma_o = 6\pi/k^2$  for  $\Delta = 0$ . After replacing these quantities into Eqs. (4) and (6), Eq. (3) yields  $S = 0$  and  $V = 1$ . Note that we have chosen  $\beta_1 = \beta_2 = \pi/2$ . We furthermore point out that  $V$  is directly related to the phase shift  $\phi$  that the scattering object induces in  $E_{\text{out}}$  [46, 47], namely

$$\phi = \arg(E_{\text{out}} E_{\text{inc}}^*) = \arg\left(1 + i\alpha \frac{cW_{\text{inc}}^{(\text{el})}(O)}{P_{\text{inc}}}\right). \quad (8)$$

We are interested in situations where the scatterer is far from being ideal, i.e. where  $\Gamma_2 \gg \Gamma_1$ . To gain insight we set  $\Delta = 0$  and write

$$\sigma_{\text{sca}} = \sigma_o (\Gamma_1/\Gamma_2)^2, \quad \sigma_{\text{ext}} = \sigma_o (\Gamma_1/\Gamma_2). \quad (9)$$

Equation (9) readily shows that  $P_{\text{sca}}$  drops more rapidly than  $P_{\text{int}}$ . That is why detection of weakly scattering objects is best achieved in extinction experiments [21, 23].

To analyze the visibility signal further, we choose a focused radially-polarized beam (FRB), because it allows a more direct comparison with nanofocusing. We remind that although  $V$  is maximal at the Bassett limit, it is only a few percents smaller for a FRB [48]. The electric field of a radially-polarized beam on the Gaussian reference sphere of an aplanatic system reads

$$E_{\text{inc}}(a, \theta) = E_o \sqrt{\cos\theta} \exp(-a^2 \sin^2 \theta / 2) a \sin\theta, \quad (10)$$

where  $E_o$  is the field amplitude,  $\theta$  is the azimuthal angle with respect to the optical axis and  $\sqrt{\cos\theta}$  is the apodization function.  $a = f/w$  is the ratio between the lens focal length  $f$  and the beam waist  $w$ .

We refer to Eq. (3) and consider full focusing and collection in the forward direction, i.e.  $\beta_1 = \beta_2 = \pi/2$ . A few algebraic steps lead to [48]

$$S = 1 - \frac{6a^4 \mathcal{I}_1^2(a, \pi/2)}{1 - (1 + a^2) \exp(-a^2)} \frac{\Gamma_1}{\Gamma_2} \left(1 - \frac{\Gamma_1}{2\Gamma_2}\right), \quad (11)$$

where  $\mathcal{I}_1(a, \beta_1)$  is the diffraction integral

$$\mathcal{I}_1(a, \beta_1) = \int_0^{\beta_1} d\theta \sin^3 \theta \sqrt{\cos\theta} \exp(-a^2 \sin^2 \theta / 2). \quad (12)$$

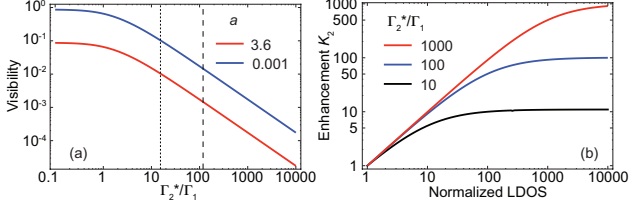


Figure 2: (a) Visibility as a function of  $\Gamma_2^*/\Gamma_1$  for two values of the beam parameter  $a$ . For  $a \rightarrow 0$  the FRB reaches its maximal focusing strength.  $a = 3.6$  corresponds to the FRB used for nanofocusing. The vertical dashed (dotted) line refers to the nanoparticle used in Fig. 5b (Fig. 5c). (b) Visibility enhancement  $K_2$  as a function of the normalized LDOS for different values of  $\Gamma_2^*/\Gamma_1$ .

Figure 2a plots  $V$  as a function of  $\Gamma_2^*/\Gamma_1$  for two values of the beam parameter  $a$ , where  $\Gamma_2 = \Gamma_1 + \Gamma_2^*$ . The curves exhibit a clear crossover between the region where radiative and non-radiative damping dominate. In the first case  $V$  is weakly dependent on  $\Gamma_2^*$  and it is only determined by the focusing strength. In the second case  $V$  drops quite rapidly and even the strongest focused beam yields a tiny signal.

By inspection of Eq. (11) we argue that  $V$  may increase up to its maximum if the radiative rate  $\Gamma_1$  be enhanced at will. Figure 2b illustrates that a change in the local density of states (LDOS) improves  $V$  by a factor

$$K_2 = \frac{F\Gamma_2}{F\Gamma_1 + \Gamma_2^*}, \quad (13)$$

where  $F$  represents the LDOS enhancement. Note that Eq. (13) is valid either for a classical oscillating dipole, where  $\Gamma_1$  and  $\Gamma_2^*$  refer to radiation and absorption, respectively, either for a quantum emitter, where  $\Gamma_1$  and  $\Gamma_2^*$  represent spontaneous emission and non-radiative decay [44]. We furthermore identify a crossover in  $K_2$  when  $F\Gamma_1$  becomes equal to  $\Gamma_2^*$ , whereby for larger  $F$  the visibility approaches its maximum and  $K_2$  saturates to  $1 + \Gamma_2^*/\Gamma_1$ .

### 2.3. Coherent scattering under nanofocusing

We are now ready to explore how nanofocusing may provide an effective way to achieve ultra-sensitive coherent detection at the nanoscale by combining large LDOS enhancements, intense near fields and a nearly background-free illumination and collection scheme.

We first recall how light propagates under nanofocusing [35, 39]. As sketched in Fig. 1b, both  $E_{\text{inc}}$  and  $E_{\text{out}}$  break the diffraction limit, because the nanocone funnels these fields to and from the probed object via the tip. A crucial feature of the configuration whereby a semi-infinite nanocone is replaced by a conical antenna is the efficient conversion between photons and SPPs. That is possible if we take a FRB and tune  $a$  (see Eq. (10)) such that the beam matches the nanocone radiation pattern. For the same purpose, the nanocone base diameter needs to be accordingly chosen [34]. When  $E_{\text{inc}}$  reaches the tip, the nanocone radius is so small that most of  $P_{\text{inc}}$  is reflected backwards [49] and it propagates towards the base, where it is radiated into the far field. Moreover, if a scatterer is placed near the tip,  $E_{\text{sca}}$  couples

to the nanocone and reaches the lens in the same spatial mode of the back-reflected  $E_{\text{inc}}$ .

Our goal is to find the detected signal  $S$ , i.e. the visibility  $V$ , and also the phase shift  $\phi$  under nanofocusing. In this derivation we assume that  $E_{\text{inc}}$  and  $E_{\text{out}}$  are perfectly converted into SPPs and vice versa, respectively. We first consider  $E_{\text{out}}$  without scatterer near the tip, as shown in Fig. 1b. In such case  $E_{\text{out}} = \kappa E_{\text{inc}}$ , where  $|\kappa| < 1$  accounts for scattering and absorption losses that occur in the nanofocusing process [50, 51].

We now add a polarizable nanoscale object near the tip. The calculation of  $E_{\text{sca}}$  requires some attention. First, in the nanofocusing process  $E_{\text{inc}}$  is enhanced by a factor  $\sqrt{|\kappa|}\xi$  with respect to the value at  $O$  in free space. Here  $\sqrt{|\kappa|}$  takes into account the effect of scattering and absorption losses in reducing the field enhancement. Second, the fraction of  $P_{\text{sca}}$  that is coupled into the nanocone is proportional to the so-called  $\beta$  factor [35]. Third, the polarizability is modified by the presence of the tip, which enhances radiation damping and leads to

$$\alpha = -\frac{6\pi}{k^3} \frac{1}{F} \frac{\Gamma_1'}{2\Delta + i\Gamma_2'}. \quad (14)$$

Here the primes indicate modified rates according to  $\Gamma_1' = F\Gamma_1$  and  $\Gamma_2' = F\Gamma_1 + \Gamma_2^*$ . Fourth, due to absorption by real metals, the fraction of  $P_{\text{sca}}$  that reaches the lens depends on  $\eta_a$ , the antenna efficiency [52]. Furthermore, for  $\Gamma_2^* \gg \Gamma_1$  we may neglect the contribution of  $\sigma_{\text{sca}}$  (see Eq. (9)). Normalizing the signal by  $|\kappa|^2 P_{\text{inc}}$  leads to

$$S \simeq 1 - \beta \frac{\eta_a}{|\kappa|} \sigma_{\text{ext}} |\xi|^2 \frac{2c W_{\text{inc}}^{(\text{el})}(O)}{P_{\text{inc}}}, \quad (15)$$

where  $W_{\text{inc}}^{(\text{el})}(O)$  has been defined in Sec. 2.1. A further simplification stems from the fact that  $\eta_a \simeq |\kappa|$ . Hence,  $V$  reads

$$V \simeq \sigma_o \frac{\beta |\xi|^2}{F} \frac{F\Gamma_1}{F\Gamma_1 + \Gamma_2^*} \frac{2c W_{\text{inc}}^{(\text{el})}(O)}{P_{\text{inc}}} = V_o \frac{\beta |\xi|^2}{F} \frac{F\Gamma_2}{F\Gamma_1 + \Gamma_2^*}, \quad (16)$$

where  $V_o$  corresponds to  $V$  under focused illumination. Recalling that  $\beta = (F - 1)/F$ , the enhancement  $K$  may be written as

$$K = K_1 K_2 = \underbrace{\frac{|\xi|^2 (F - 1)}{F^2}}_{K_1} \underbrace{\frac{F\Gamma_2}{F\Gamma_1 + \Gamma_2^*}}_{K_2} \quad (17)$$

A similar expression is obtained when  $\Gamma_2^*$  is due to elastic processes (dephasing). Equation (17) reveals that  $V$  improves by two mechanisms. Besides the one discussed in the previous section, which we named  $K_2$ , we note an additional term  $K_1$  that depends on  $|\xi|^2$  and  $F$ . For  $F \gg 1$ ,  $\beta$  is close to one and  $K_1$  reduces to  $|\xi|^2/F$ . While for resonant dipole antennas it is common to find  $|\xi|^2 < F$ , for nanofocusing we may have the opposite result. That is possible because the incident beam is weakly focused (see Fig. 2a).

At last, we wish to examine the role of  $\kappa$  and  $\eta_a$ . Although they do not appear in Eq. (16), they are nevertheless important as the output signal is proportional to  $|\kappa|^2$  and  $|\kappa|\eta_a$ . Indeed, if  $\kappa$  tends to zero the amount of power that reaches the tip becomes negligible. Likewise if  $\eta_a$  is very small most of  $P_{\text{sca}}$  gets

absorbed in the nanocone. Thus the whole enhancement process is meaningless, because it is given by the division of two vanishing signals, namely  $|\kappa|^2 P_{\text{inc}}$  and  $\eta_a |\kappa| P_{\text{sca}}$ . It is therefore crucial to operate with antenna architectures that combine huge LDOS enhancements with moderate absorption losses.

### 3. Results

#### 3.1. Metal nanocones

We have modeled gold nanocones using a body-of-revolution (BOR) finite-difference time-domain (FDTD) approach [53]. Figure 3a sketches a nanocone attached to an AFM cantilever, treated as a semi-infinite quartz substrate. We have considered nanocone lengths between 1000 and 3000 nm, and base diameters optimized according to the wavelength range of interest [34]. Without loss of generality we choose to work around 740 nm, which corresponds to an optimal base radius of 195 nm. The tip has a radius of curvature of 5 nm, which is a realistic value for state of the art nanofabrication [36]. If not otherwise stated, the FDTD mesh has a discretization of 1 nm.

We now move to the input and output fields. We illuminate the nanocone using a FRB with  $a = 3.6$  to optimize the conversion of photons into SPPs. Figure 3b shows the magnetic field amplitude as the wave propagates towards the tip and comes back. A standing-wave pattern is indeed clearly visible. Moreover, note that its structure changes as the field approaches the tip, because the effective wavelength becomes shorter in the nanofocusing process [38, 39]. We have calculated how much power is absorbed by a 2000 nm long gold nanocone, finding that it amounts to nearly 50% of  $P_{\text{inc}}$ , hence  $|\kappa|^2 = 0.5$ . Figure 3c plots the absorbed power  $P_{\text{abs}}$  and the output power  $P_{\text{out}}$  as a function of wavelength. Note that  $P_{\text{out}}$  is in fact a little less than  $P_{\text{inc}} - P_{\text{abs}}$ , because scattering losses occur during nanofocusing and conversion of SPPs.

Next we introduce  $E_{\text{sca}}$  by placing an oscillating dipole 10 nm from the tip, oriented along the optical axis. Figure 3d confirms that most of the power is radiated along the nanocone and exits the other end with an efficiency  $\eta_a$  of about 70%, which is consistent with  $\eta_a \simeq |\kappa|$ . To explore how  $E_{\text{sca}}$  behaves in the far field, we have performed a near-to-far field transformation. The result is plotted in Fig. 3e for different nanocone lengths. As the nanocone gets longer the far field approaches that of a metal nanowire, indicated by a dotted curve. The dashed curve shows instead the profile of a FRB for  $a = 3.6$ . We find that  $a$  needs to be adjusted to optimize the coupling also in relation to the nanocone length. In practice, a shorter nanocone requires a FRB with a slightly smaller  $a$ . Note that the length is an important parameter as it determines nanofocusing strength and propagation losses, which also depend on the nanocone composition and working wavelength [50, 51].

Having analyzed the behavior of the input and output fields, we move our attention to the enhancement factors. These are plotted in Fig. 4a, which shows  $|\xi|^2$  and  $F$  as a function of distance from the tip. Both intensity and LDOS enhancements are strongly distance dependent and grow very rapidly as we approach the tip.

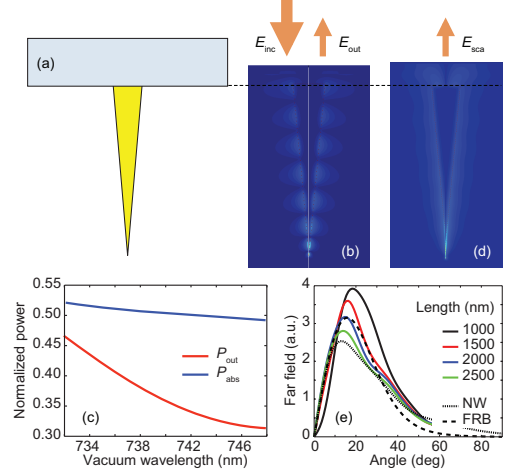


Figure 3: (a) Sketch of a nanocone mounted on a quartz AFM cantilever. The nanocone has a base radius of 195 nm and a tip radius of 5 nm. Its height is 2000 nm. (b)  $E_{\text{inc}}$  and  $E_{\text{out}}$  without sample near the tip. (c)  $P_{\text{out}}$  and  $P_{\text{abs}}$  normalized with respect to  $P_{\text{inc}}$ . (d)  $E_{\text{sca}}$  generated by an oscillating dipole placed 10 nm from the tip. In (b) and (d) the field patterns represent the magnetic field amplitude at 740 nm. (e) Far field as a function of the nanocone length at 740 nm. The dashed and dotted curves respectively refer to the far field of a FRB with  $a = 3.6$  and a gold nanowire (NW). The base and tip radii are like in (a) for all lengths.

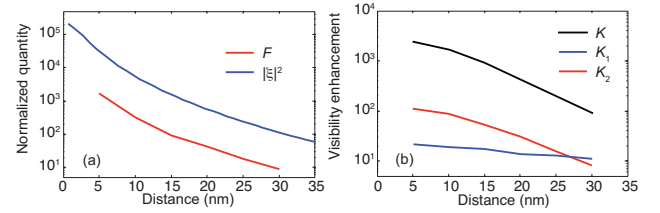


Figure 4: (a) Intensity enhancement  $|\xi|^2$ , normalized LDOS  $F$  and (b) visibility enhancement  $K$  as a function of distance. The individual contributions  $K_1$  and  $K_2$  are also indicated. For the beam and nanocone parameters see Fig. 3.  $\Gamma_2^*/\Gamma_1$  is equal to 119, which corresponds to the nanoparticle discussed in Fig. 5b.

We are ready to quantify the visibility enhancements  $K_1$  and  $K_2$ , which are shown Fig. 4b for  $\Gamma_2^*/\Gamma_1 \simeq 100$ . We remark that  $K_1$  is independent of  $\Gamma_2^*/\Gamma_1$  as it contains only  $|\xi|^2$  and  $F$ . Furthermore, it weakly depends on the distance from the tip. On the other hand,  $K_2$  changes by more than one order of magnitude as the distance is reduced by a few tens of nanometers. Moreover, it approaches a plateau for distances less than 10 nm. There,  $F$  becomes larger than  $\Gamma_2^*/\Gamma_1$  and  $K_2$  saturates to its maximum (see Fig. 2b). The cooperation of  $K_1$  and  $K_2$  leads to an overall enhancement of more than three orders of magnitude.

#### 3.2. Metal nanoparticles

We verify our findings by performing coherent spectroscopy on very small metal particles. To gain insight we treat them as a point-like oscillating dipole with radiative corrections [54], whose polarizability reads

$$\alpha \simeq -4\pi r^3 \frac{\omega_o}{2\Delta + i(\gamma + 2\omega_o(kr)^3/3)}, \quad (18)$$

where  $r$  is the nanoparticle radius. This expression is analogous to Eq. (2). We have used the Drude model to describe

the nanosphere dielectric function  $\epsilon(\omega) = 1 - \omega_p^2 / (\omega(\omega + i\gamma))$ , where  $\omega_p$  and  $\gamma$  are the so-called plasma and damping frequencies [55]. In Eq. (18)  $\omega_o$  stands for  $\omega_p / \sqrt{3}$ .

$\Gamma_2^*$  represents material losses in the metal nanosphere and it corresponds to  $\gamma$ . Radiation losses are instead parametrized by  $(kr)^3$ . A few algebraic steps lead to

$$\frac{\Gamma_2^*}{\Gamma_1} = \frac{\gamma}{\omega_p} \frac{3\sqrt{3}}{2(kr)^3}. \quad (19)$$

Although  $\gamma/\omega_p$  is commonly much smaller than one, the possibility that  $kr \ll 1$  may lead to substantial quenching of radiative damping and to a considerable increase of  $\Gamma_2^*/\Gamma_1$ .

The strength of light-matter interaction gets smaller due to a decrease in the polarizability (see Eq. (18)). Moreover, the nanoparticle absorbs most of the light that is coupled to it. To study how these phenomena affect  $V$ , we respectively introduce the nanoparticle and the scattering efficiencies [48],

$$\eta_{NP} = \frac{\sigma_{ext}}{\sigma_o} = \frac{k^3 \text{Im}(\alpha)}{6\pi}, \quad \eta_{sca} = \frac{\sigma_{sca}}{\sigma_{ext}} = \frac{k^3 |\alpha|^2}{6\pi \text{Im}(\alpha)}, \quad (20)$$

which turn out to be

$$\eta_{NP} = \eta_{sca} = \left(1 + \frac{\Gamma_2^*}{\Gamma_1}\right)^{-1}. \quad (21)$$

For our analysis we set  $\gamma/\omega_p = 0.001$  and two different nanoparticle radii, namely 2.5 and 5 nm. Moreover, we choose  $\omega_p$  such that the resonance wavelength is 675 nm and 740 nm, respectively. These parameters lead to  $\Gamma_2^*/\Gamma_1 \simeq 119$  for  $r = 2.5$  nm and  $\Gamma_2^*/\Gamma_1 \simeq 16$  for  $r = 5$  nm. The corresponding  $V$  under focusing is marked by vertical lines in Fig. 2a. It amounts to 1-10% for the strongest focused beam and to 0.1-1% for the FRB used for nanofocusing.

### 3.3. Visibility and phase shift under nanofocusing

To facilitate the FDTD calculations we have reduced the nanocone length to 1000 nm and increased the mesh pitch to 2 nm. While the latter may reduce the accuracy of our results, it does not fake the main effect that we are interested in, namely the enhancement of  $V$ . The layout of the problem is sketched in Fig. 5a.

Figures 5b and 5c show that  $V$  up to 83% may be achieved if the nanoparticle is probed by a nanofocused beam. In comparison to the curve in Fig. 2a, it corresponds to enhancements of more than two orders of magnitude. As expected, to achieve the same signal with the smaller object we need to operate at shorter distances. As the nanocone approaches the nanosphere we recognize an increase in radiative damping by broadening of the dip in  $P_{out}$ . Note that  $P_{out}$  without nanoparticle is about 44%, in agreement with the result of Fig. 3d, which refers to a nanocone length of 2000 nm. The enhancement of light-matter interaction is noticeable in the phase shift too, which is plotted in Fig. 5d. We finally remark that  $K$  may be further improved by optimizing the nanocone parameters [50, 51], reducing the working distance and choosing systems with larger  $\Gamma_2^*/\Gamma_1$ .

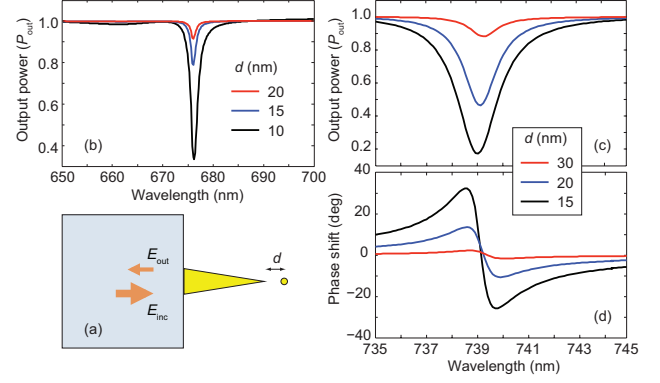


Figure 5: (a) Layout of the scattering problem (nanoparticle not to scale). Signal ((b) and (c)) and phase shift (d) as a function of wavelength for various distances from the tip. The nanoparticle radius is 2.5 nm (b) or 5 nm ((c) and (d)) (see text for details).

## 4. Conclusions

We have proposed an implementation of coherent optical nanoscopy based on the nanofocusing concept and on scanning-probe technology. We have discussed the basic principles of this method and its potential in enhancing the detection of nanoscale objects. We have identified the two mechanisms that increase  $V$ , namely the intensity enhancement and the modification of the LDOS at the nanocone sharp end. While the second effect has been first investigated in single-molecule SNOM [56, 57] and more recently in quantum-optics [35], here we have shown how it may increase the visibility and the phase shift caused by an oscillating dipole.

In comparison with grating coupled nanofocusing [58], which also provides a nanoscale source for scattering-type SNOM [59, 60], our approach exploits nanofocusing in both illumination and collection channels and realizes a kind of  $4\pi$  optical system. That is not easy to implement with grating couplers, because the throughput may not be high enough.

In comparison with resonant optical antennas, whereby coherent coupling has been studied from a quantum-optical perspective [61], our scheme does not suffer from resonance shifts that occur when a nano-emitter approaches the antenna [62]. We remark that these may completely detune the antenna and compromise the enhancements.

We wish to emphasize that these concepts are readily extendible to ultrafast and nonlinear techniques [63–67], as well as coherent control [68], whereby short laser pulses are efficiently converted into SPPs and nanofocused. Multidimensional correlation spectroscopies [69] may also be implemented at the nanoscale in this way, without the need for hybrid approaches [70]. Lastly, we wish to point out that these ideas may also be pursued in the infrared spectral range using surface phonon-polaritons [71] or at THz and lower frequencies using spoof SPPs [72, 73].

## Acknowledgments

A. Mohammadi is thankful to the Persian Gulf University Research Council for continuous support. M. Agio wish to thank



Vahid Sandoghdar for advice and encouragement and Xuwen Chen for fruitful discussions.

## References

- [1] D. W. Pohl, W. Denk, M. Lanz, *Appl. Phys. Lett.* 44 (1984) 651–653.
- [2] A. Lewis, M. Isaacson, A. Harootunian, A. Muray, *Ultramicroscopy* 13 (1984) 227–231.
- [3] Y. Inouye, S. Kawata, *Opt. Lett.* 19 (1994) 159–161.
- [4] A. Hartschuh, *Angew. Chem. Int. Ed.* 47 (2008) 8178–8191.
- [5] E. Betzig, J. K. Trautman, *Science* 257 (1992) 189–195.
- [6] X. S. Xie, J. K. Trautman, *Annu. Rev. Phys. Chem.* 49 (1998) 441–480.
- [7] S. Weiss, *Science* 283 (1999) 1676–1683.
- [8] W. E. Moerner, *J. Phys. Chem. B* 106 (2002) 910927.
- [9] J. M. Lupton, *Adv. Mater.* 22 (2010) 1689–1721.
- [10] M. Orrit, J. Bernard, *Phys. Rev. Lett.* 65 (1990) 2716–2719.
- [11] W. E. Moerner, T. Plakhotnik, T. Irngartinger, U. P. Wild, D. W. Pohl, B. Hecht, *Phys. Rev. Lett.* 73 (1994) 2764–2767.
- [12] H. F. Hess, E. Betzig, T. D. Harris, L. N. Pfeiffer, K. W. West, *Science* 264 (1994) 1740–1745.
- [13] J. K. Trautman, J. J. Macklin, L. E. Brus, E. Betzig, *Nature* 369 (1994) 40–42.
- [14] E. Betzig, R. J. Chichester, *Science* 262 (1993) 1422–1425.
- [15] A. A. Mikhailovsky, M. A. Petruska, M. I. Stockman, V. I. Klimov, *Opt. Lett.* 28 (2003) 1686–1688.
- [16] W. E. Moerner, L. Kador, *Phys. Rev. Lett.* 62 (1989) 2535–2538.
- [17] F. Zenhausern, Y. Martin, H. K. Wickramasinghe, *Science* 269 (1995) 1083–1085.
- [18] L. Kador, T. Latychevskaya, A. Renn, U. P. Wild, *J. Chem. Phys.* 111 (1999) 8755–8758.
- [19] I. Gerhardt, G. Wrigge, P. Bushev, G. Zumofen, M. Agio, R. Pfab, V. Sandoghdar, *Phys. Rev. Lett.* 98 (2007) 033601.
- [20] G. Wrigge, I. Gerhardt, J. Hwang, G. Zumofen, V. Sandoghdar, *Nat. Phys.* 4 (2008) 60–66.
- [21] P. Kukura, M. Celebrano, A. Renn, V. Sandoghdar, *J. Phys. Chem. Lett.* 1 (2010) 3323–3327.
- [22] M. Pototschnig, Y. Chassagneux, J. Hwang, G. Zumofen, A. Renn, V. Sandoghdar, *Phys. Rev. Lett.* 107 (2011) 063001.
- [23] M. Celebrano, P. Kukura, A. Renn, V. Sandoghdar, *Nat. Photon.* 5 (2011) 95–98.
- [24] G. Zumofen, N. M. Mojarad, V. Sandoghdar, M. Agio, *Phys. Rev. Lett.* 101 (2008) 180404.
- [25] N. M. Mojarad, G. Zumofen, V. Sandoghdar, M. Agio, *J. Eur. Opt. Soc.: RP* 4 (2009) 09014.
- [26] J.-J. Greffet, *Science* 308 (2005) 1561–1563.
- [27] P. Mühlischlegel, H.-J. Eisler, O. J. F. Martin, B. Hecht, D. W. Pohl, *Science* 308 (2005) 1607–1609.
- [28] L. Novotny, N. van Hulst, *Nat. Photon.* 5 (2011) 83–90.
- [29] P. Anger, P. Bharadwaj, L. Novotny, *Phys. Rev. Lett.* 96 (2006) 113002.
- [30] S. Kühn, U. Håkanson, L. Rogobete, V. Sandoghdar, *Phys. Rev. Lett.* 97 (2006) 017402.
- [31] S. Kühn, G. Mori, M. Agio, V. Sandoghdar, *Mol. Phys.* 106 (2008) 893–908.
- [32] T. H. Taminiau, F. D. Stefani, F. B. Segerink, N. F. van Hulst, *Nat. Photon.* 2 (2008) 234–237.
- [33] A. G. Curto, G. Volpe, T. H. Taminiau, M. P. Kreuzer, R. Quidant, N. F. van Hulst, *Science* 329 (2010) 930–933.
- [34] X.-W. Chen, V. Sandoghdar, M. Agio, *Opt. Express* 18 (2010) 10878–10887.
- [35] D. E. Chang, A. S. Sørensen, P. R. Hemmer, M. D. Lukin, *Phys. Rev. Lett.* 97 (2006) 053002.
- [36] F. De Angelis, G. Das, P. Candeloro, M. Patrini, M. Galli, A. Bek, M. Lazzarino, I. Maksymov, C. Liberale, L. C. Andreani, E. Di Fabrizio, *Nat. Nano.* 5 (2010) 67–72.
- [37] J. Takahara, S. Yamagishi, H. Taki, A. Morimoto, T. Kobayashi, *Opt. Lett.* 22 (1997) 475–477.
- [38] A. J. Babadjanyan, N. L. Margaryan, K. V. Nerkararyan, *J. Appl. Phys.* 87 (2000) 3785–3788.
- [39] M. I. Stockman, *Phys. Rev. Lett.* 93 (2004) 137404.
- [40] D. K. Gramotnev, S. I. Bozhevolnyi, *Nat. Photon.* 4 (2010) 83–91.
- [41] C. F. Bohren, D. R. Huffman, *Absorption and Scattering of Light by Small Particles*, John Wiley & Sons, New York, 1983.
- [42] J. A. Lock, J. T. Hodges, G. Gouesbet, *J. Opt. Soc. Am. A* 12 (1995) 2708–2715.
- [43] J. D. Jackson, *Classical Electrodynamics*, John Wiley & Sons, New York, third edition, 1999.
- [44] L. Allen, J. Eberly, *Optical resonance and two-level atoms*, Dover, New York, 1975.
- [45] I. M. Bassett, *Optica Acta* 33 (1986) 279–286.
- [46] G. Zumofen, N. M. Mojarad, M. Agio, *N. Cimento C* 31 (2009) 475–485.
- [47] S. A. Aljunid, M. K. Tey, B. Chng, T. Liew, G. Maslennikov, V. Scarani, C. Kurtsiefer, *Phys. Rev. Lett.* 103 (2009) 153601.
- [48] M. Agio, G. Zumofen, N. M. Mojarad, V. Sandoghdar, in: S. Kawata, V. M. Shalae, D. P. Tsai (Eds.), *Plasmonics: Nanoimaging, Nanofabrication, and their Applications V*, volume 7395, Proc. SPIE, 2009, p. 739512.
- [49] R. Gordon, *Opt. Express* 17 (2009) 18621–18629.
- [50] M. W. Vogel, D. K. Gramotnev, *Phys. Lett. A* 363 (2007) 507–511.
- [51] D. K. Gramotnev, M. W. Vogel, M. I. Stockman, *J. Appl. Phys.* 104 (2008) 034311.
- [52] L. Rogobete, F. Kaminski, M. Agio, V. Sandoghdar, *Opt. Lett.* 32 (2007) 1623–1625.
- [53] A. Taflove, S. C. Hagness, *Computational Electrodynamics: The Finite-Difference Time-Domain Method*, Artech House, Norwood, MA, third edition, 2005.
- [54] A. Wokaun, J. P. Gordon, P. F. Liao, *Phys. Rev. Lett.* 48 (1982) 957–960.
- [55] N. W. Ashcroft, N. D. Mermin, *Solid State Physics*, Saunders College Publishing, Fort Worth, 1976.
- [56] W. P. Ambrose, P. M. Goodwin, R. A. Keller, J. C. Martin, *Science* 265 (1994) 364–367.
- [57] R. X. Bian, R. C. Dunn, X. S. Xie, P. T. Leung, *Phys. Rev. Lett.* 75 (1995) 4772–4775.
- [58] C. Ropers, C. C. Neacsu, T. Elsaesser, M. Albrecht, M. B. Raschke, C. Lienau, *Nano Lett.* 7 (2007) 2784–2788.
- [59] C. Neacsu, S. Berweger, R. Olmon, L. Saraf, C. Ropers, M. Raschke, *Nano Lett.* 10 (2010) 592–596.
- [60] D. Sadiq, J. Shirdel, J. Lee, E. Selishcheva, N. Park, C. Lienau, *Nano Lett.* 11 (2011) 1609–1613.
- [61] A. Ridolfo, O. Di Stefano, N. Fina, R. Saija, S. Savasta, *Phys. Rev. Lett.* 105 (2010) 263601.
- [62] Y. Alavverdyan, N. Vamivakas, J. Barnes, C. Leboutteiller, J. Hare, M. Atatüre, *Opt. Express* 19 (2011) 18175–18181.
- [63] E. J. Sánchez, L. Novotny, X. S. Xie, *Phys. Rev. Lett.* 82 (1999) 4014–4017.
- [64] T. Guenther, C. Lienau, T. Elsaesser, M. Glanemann, V. M. Axt, T. Kuhn, S. Eshlaghi, A. D. Wieck, *Phys. Rev. Lett.* 89 (2002) 057401.
- [65] T. Ichimura, N. Hayazawa, M. Hashimoto, Y. Inouye, S. Kawata, *Phys. Rev. Lett.* 92 (2004) 220801.
- [66] M. Celebrano, P. Biagioni, M. Zavelani-Rossi, D. Polli, M. Labardi, M. Allegrini, M. Finazzi, L. Duò, G. Cerullo, *Rev. Sci. Instr.* 80 (2009) 033704.
- [67] S. Berweger, J. M. Atkin, X. G. Xu, R. L. Olmon, M. B. Raschke, *Nano Lett.* 11 (2011) 4309–4313.
- [68] D. Brinks, F. D. Stefani, F. Kulzer, R. Hildner, T. H. Taminiau, Y. Avlasevich, K. Mullen, N. F. van Hulst, *Nature* 465 (2010) 905–908.
- [69] S. Mukamel, *Annu. Rev. Phys. Chem.* 51 (2000) 691–729.
- [70] M. Aeschlimann, T. Brixner, A. Fischer, C. Kramer, P. Melchior, W. Pfeiffer, C. Schneider, C. Strber, P. Tuchscherer, D. V. Voronine, *Science* (2011).
- [71] R. Hillenbrand, T. Taubner, F. Keilmann, *Nature* 418 (2002) 159–162.
- [72] S. A. Maier, S. R. Andrews, L. Martín-Moreno, F. J. García-Vidal, *Phys. Rev. Lett.* 97 (2006) 176805.
- [73] G. Goubau, *J. Appl. Phys.* 21 (1950) 1119–1128.